Two-Dimensional Adaptive Mesh Generation Algorithm and its Application with Higher-Order Compressible Flow Solver

Sutthisak Phongthanapanich, Pramote Dechaumphai*
Mechanical Engineering Department, Chulalongkorn University, Bangkok 10330, Thailand

A combined procedure for two-dimensional Delaunay mesh generation algorithm and an adaptive remeshing technique with higher-order compressible flow solver is presented. A pseudo-code procedure is described for the adaptive remeshing technique. The flux-difference splitting scheme with a modified multidimensional dissipation for high-speed compressible flow analysis on unstructured meshes is proposed. The scheme eliminates nonphysical flow solutions such as the spurious bump of the carbuncle phenomenon observed from the bow shock of the flow over a blunt body and the oscillation in the odd-even grid perturbation in a straight duct for the Quirk's odd-even decoupling test. The proposed scheme is further extended to achieve higher-order spatial and temporal solution accuracy. The performance of the combined procedure is evaluated on unstructured triangular meshes by solving several steady-state and transient high-speed compressible flow problems.

Key Words: Adaptive Mesh, Delaunay Triangulation, Carbuncle Phenomenon, H-correction Entropy Fix

1. Introduction

Spatial discretization of a given domain is a prerequisite for solutions with finite-element or finite-volume method of a partial differential equations system that represents the physical model of the problem. Generally, triangulation process starts from the generation of the point list; the points are subsequently connected into triangular elements. The points connection step is often performed by constructing the Delaunay triangulation (Bowyer, 1981; Watson, 1981) of the point set to guarantee triangles which are as well-shaped as possible for the given points. Since the Delaunay triangulation in itself does not include procedures for creating points inside the domain, points are generated independently by an automatic point creation algorithm (Marchant and Weatherill, 1993; Karamete et al., 1997).

To enhance the solution accuracy of the numerical analysis and to improve the computed solution, mesh adaptation is needed. An adaptive remeshing technique is incorporated with an appropriated error indicator to dictate a close correlation between the size of elements and the behavior of the corresponding computed solution. The technique is implemented to capture the fast variation of the solution with a reasonable number of elements. The process of the adaptive meshing is to first generate an initial mesh for the domain. The mesh is used to compute the corresponding solution by the finite-element or finite-volume method. Then the regions where adaptation is vital are determined by an error indicator, and new adapted mesh for the solution is entirely generated. The same process is repeated until the specified convergence criterion is met. The efficiency of the overall

* Corresponding Author,
E-mail: fmepdc@eng.chula.ac.th
Mechanical Engineering Department, Chulalongkorn University, Bangkok 10330, Thailand. (Manuscript **Received** May 25, 2004; **Revised** September 23, 2004)

procedure is evaluated by calculating flows that include the supersonic shock waves and shock propagation behaviors.

High-speed compressible flows normally involve complex flow phenomena, such as strong shock waves and shock-shock interactions. Various numerical inviscid flux formulations have been proposed to solve an approximate Riemann problem (Roe, 1981 ; Steger and Warming, 1981 ; Liou et al., 1993 ; Toro et al., 1994 ; Kang et al., 2002 ; Kang et al., 2003). Among these formulations, the flux-difference splitting scheme by Roe (1981) is widely used due to its accuracy, quality and mathematical clarity. However, the scheme may sometimes lead to nonphysical flow solutions in certain problems, such as the carbuncle phenomenon (Perry and Imlay, 1988) with a spurious bump in the bow shock for flow over a blunt body. In the odd-even decoupling problem (Quirk, 1994), an unrealistic perturbation may grow with the planar shock as it moves along the duct. To improve the solution accuracy of these problems, Quirk pointed out that the original Roe's scheme should be modified or replaced by other schemes in the vicinity of strong shock. It has been known that the original Roe's scheme does not satisfy the entropy condition and may allow unrealistic expansion shock. Harten (1983) proposed an entropy fix formulation to replace the near zero small eigenvalues by some tolerances. The mathematical background of the Harten's entropy fix with the suggested tolerance values is given by Van Leer et al.(1989).

This paper proposed a mixed entropy fix method for the Roe's scheme on adaptive unstructured meshes for two-dimensional high-speed compressible flow analysis. The entropy fix method by Van Leer et al. and the multidimensional dissipation technique of Pandolfi and D'Ambrosio (2001) are modified for unstructured triangular meshes and implemented into the original Roe's scheme. The presented scheme is further extended to higher-order solution accuracy and then evaluated by several benchmark test cases.

The presentation in this paper starts at Section 2 describing an adaptive remeshing technique with the implementation procedure in an objected-oriented programming concept. Section 3 describes the Roe's flux-difference splitting scheme with some well-known problems that exhibit numerical shock instability. A Roe's scheme with a mixed entropy fix method is then proposed and examined for their capabilities. The presented scheme is further extended to higher-order solution accuracy and then evaluated by several benchmark test cases in Section 4. Finally, the performance of the scheme is evaluated on adaptive unstructured meshes for solving both the steady-state and transient high-speed compressible flow problems.

2. Delaunay Triangulation and Adaptation Technique

2.1 Mesh generation and adaptation

The mesh generation implemented in this paper follows the Delaunay triangulation (Bowyer, 1981 ; Watson, 1981). The algorithm itself does not provide the procedure for creating new points inside the domain. The automatic point creation procedure presented in this paper are derived from the algorithm suggested by Marchant and Weatherill (1993). The shape and size of elements or density of points inside the domain are controlled by two coefficients, the Alpha and the Beta coefficients. The main idea of the automatic point creation procedure is to search for the element that conforms to both the Alpha and Beta testing criteria and a new point placement at the centroid of that element. New elements can then be created by the Delaunay triangulation algorithm. The step-by-step explanation of these algorithms was presented in detail in Ref.(Phongthanapanich and Dechaumphai, 2004).

To capture fast variations of the solution, small elements are needed along that region in the domain. The proper element size h_i is computed by requiring that the error should be uniform for all elements (Dechaumphai and Morgan, 1992):

$$h_i^2\lambda_i = h_{\min}^2\lambda_{\max} = \text{constant} \qquad (1)$$

where λi is the higher principal quantity of the element considered,

$$\lambda_i=\max\left(\left|\frac{\partial^2\phi}{\partial X^2}\right|,\left|\frac{\partial^2\phi}{\partial Y^2}\right|\right) \quad (2)$$

and ϕ is the selected solution indicator. In the above Eq. (1), λ_{max} is the maximum principal quantity for all elements and h_{min} is the minimum element size specified by users. The regions, which will be refined or coarsened by Adaptive-Remeshing algorithm below, are identified by a dimensionless error indicator using the pressure-switch coefficient (Probert et al., 1991). The indicator at node I is given by,

$$E_I=\frac{\sum_{e\in I}|2\phi_I-\phi_J-\phi_K|}{\sum_{e\in I}(A^*+B^*)} \quad (3)$$

where J and K are the other two nodes of the triangle, e, $A^*=\max(|\phi_I-\phi_J|, \alpha(\phi_I+\phi_J))$ and $B^*=\max(|\phi_I-\phi_K|, \alpha(\phi_I+\phi_K))$. The value of α is used to identify the solution discontinuity or numerical oscillation. According to numerical experiment especially for the proposed scheme that will be explained later, the value of α is prescribed as 0.005 in this paper. This means $A^*=0.005(\phi_I+\phi_J)$ and $B^*=0.005(\phi_I+\phi_K)$ if ϕ_J and ϕ_K are oscillated within 1% of ϕ_I, respectively.

Practical experience found that this type of error indicator for the transient high-speed compressible flow problems, where regions such as shock or discontinuity have different strength, may cause inaccurate solution due to the inadequate refinement because the point spacing is scaled according to the maximum value of the second derivatives. In order to overcome this problem, an element size scaling function, which scales the point spacing of point p_i within the range of χ_{min} and χ_{max}, has been used:

$$\chi_i=\text{scaleRange}\left(\frac{h_{max}-dp_i}{h_{max}-h_{min}},\ 0,\ 1,\ \chi_{min},\ \chi_{max}\right) \quad (4)$$

The coefficient χ_i controls the point insertion in the regions of high solution gradient and eliminates excessive distortion of the regularity of the triangulation. The value of χ_{min} limits the number of points insertion in the high gradient region such as shock, while the value of upper limit χ_{max} allows to insert more points into the region with smaller solution gradient such as the tail of the expansion fan. When the adapted elements generated by this function are distorted in shape, the Alpha and Beta coefficients are incorporated to control the point density and the regularity of triangulation.

The proposed adaptive mesh regeneration is based on the concepts of the Delaunay triangulation and the mesh refinement. The new mesh is constructed using the information from the previous or background mesh, and it is composed of small elements in the regions with large changes of the solution gradients, and large elements in the remaining regions where the changes of the solution gradients are small. Detailed process of adaptive remeshing technique is described as follows.

Algorithm AdaptiveRemeshing (*P, T, P0, alpha, beta, h_{min}, h_{max}, Xi_{min}, Xi_{max}, threshold*)

1. Let $P0$, $k=1, \cdots, n$ be the set of points of the background mesh.
2. Let P be the set of points and T be the set of triangles.
3. Read next interior point p_i of the background mesh from $P0$.
4. If $h_i>h_{max}$ then go to step 3.
5. Search triangle t_i in T which contains the point p_i. Then calculate the centroid of the triangle t_i and define it as point p_q, and compute the point distribution function of point p_q by Eq. (5).

$$dp_q=\frac{1}{M}\sum_{j=1}^{M}|p_j-p_q| \quad (5)$$

where M is number of surrounding nodes to node q.

6. Compute the distance d_m, $m=1, 2, 3$ from point pq to each of the three vertices of the triangle t_i.
7. Compute the Xi coefficient, χ_i, for point p_i by using Eq. (4), and the average distance, $s_i=(d_1+d_2+d_3)/3$.
8. Perform the Xi-Alpha test for point p_q. If $(\chi_i*alpha*h_i)>=s_i$, then reject the point p_q and return to step 3.
9. Perform the Xi-Beta test for point p_q. If two out of three of $d_m<(\chi_i*h_{min}/beta)$ for any

$m=1, 2, 3$, then reject the point p_q and return to step 3.

10. Accept the point p_q for insertion by the Delaunay triangulation algorithm and add point p_q into P.

11. Repeat steps 3 to 10 until all points in P are considered.

12. Perform the Delaunay triangulation of the inserted points in P.

13. If number of accepted points greater than threshold, then go to step 3; otherwise stop the algorithm.

Since the proposed algorithm above does not guarantee the good mesh topology, the mesh relaxation (Frey, 1991) based on an edge-swapping technique is highly recommended for well-shaped mesh improvement. The objective of this method is to make the topology of elements closer to equilateral triangles by swapping edges to equalize the vertex degrees (number of edges linked to each point) toward the value of six. Finally, the Laplacian smoothing is applied to smooth the meshes.

2.2 Mesh generation implementation and algorithm evaluation

This section presents the main algorithm for combining together the mesh generation from the Delaunay triangulation, the mesh refinement procedure, and the adaptive remeshing technique. This main algorithm is demonstrated using the object-oriented programming concept that takes into account the advantages of the code encapsulation, inheritance, and polymorphism capabilities. The implementation of the main algorithm is summarized in the algorithm below.

Algorithm **Main**
(*P, T, alpha, beta, iteration,* H_{min}, H_{max}, $\_Xi\_{min}$, Xi_{max}, *threshold, isadaptive*)
Let *BP* be the collection of boundary point objects that stored in sequence of counter-clockwise direction for all outside boundaries and clockwise direction for all inside boundaries;
Let *P0* be the collection of background point objects;
Let *P* be the collection of point objects;
Let *T* be the collection of mesh objects;
Let *alpha* be the constant that controls shape of formed triangles;
Let *beta* be the constant that controls regularity of the triangulation;
Let *iteration* be the number of loops to refine meshes;
Let H_{min} and H_{max} be the minimum and maximum element size, respectively;
Let Xi_{min} and Xi_{max} be the minimum and maximum scaling coefficients, respectively;
Let *threshold* be the number of minimum increasing points for each iteration;
Let *isadaptive* be the flag to generate background or adaptive meshes;

```
Bp. Initialize;
P0. Initialize;
P. Initialize;
T. Initialize;
If. (isadaptive) {
   P0. ReadBackgroundNodes;
   BP. RediscretizeBoundaryNodes;
   };
Else {
   BP. ReadBoundaryNodes;
};
BP. CreateConvexHull;
P. AddNode (BP. p1, BP. p2, BP. p3, BP. p4);
T. AddTriangle (t1, BP. p1, BP. p2, BP. p3);
T. AddTriangle (t2, BP. p3, BP. p2, BP. p4);

Do p ← BP. NextBoundaryNode {
   Call DelaunayTriangulation (P, T, p);
};
T. RemoveOutsideDomainTriangles;

Call MeshRefinement
      (P, T, alpha, beta, iteration);
If (isadaptive)
   Call AdaptiveRemeshing
      (P, T, P0, alpha, beta, Hmin, Hmax, _Xi_min,
      Xi_max, threshold);

T. MeshRelaxation;
T. LaplaceSmoothing;
End;
```

To evaluate the performance of the adaptive remeshing technique with the Delaunay triangulation, the specification of element size, h_i, is given as an analytic function defined for two-dimensional domain. The adaptive mesh generation process starts from an initial mesh generated in the domain, then the values of the element sizes at all points are computed by the given function. The mesh generation coupled with the adaptive remeshing procedure is iterated until the resulting mesh becomes globally stable. The iteration process is terminated if the total node increment is fewer than the specified number. The three examples of adaptive mesh generation with the analytical function for specifying element sizes presented herein are: (1) adaptive meshes along the centerline of a rectangular domain, (2) adaptive meshes along the diagonal of a square domain, and (3) an alpha-shape adaptive meshes in a square domain.

Adaptive Meshes along Centerline of a Rectangular Domain: The first example presents an adaptive mesh generation in a 3.0×5.0 rectangular domain. The element sizes at points in the domain are given by the distribution function,

$$h(y)=0.42-\frac{1}{\sqrt{2\pi}\sigma}e^{-\left[\frac{y-\mu}{2\sigma}\right]^2} \qquad (6)$$

where y is the variable and the values of μ and σ are constants equal to zero and one, respectively. Figure 1 shows the series of adaptive meshes generated by three iterations based on a coarse initial mesh. The value of mesh generation coefficients, α, β, χ_{min}, χ_{max} are 0.5, 0.6, 0.75, and 1.10, respectively. Due to the prescribed distribution function in Eq. (6), small element sizes are specified around the centerline of the domain. The figure shows that size similarity of the adaptive meshes is generated along the narrow band around the centerline of the domain. The value of χ_{min} limits the number of point insertion along the centerline of the domain, while the value of χ_{max} allows more nodes to be inserted into the other regions.

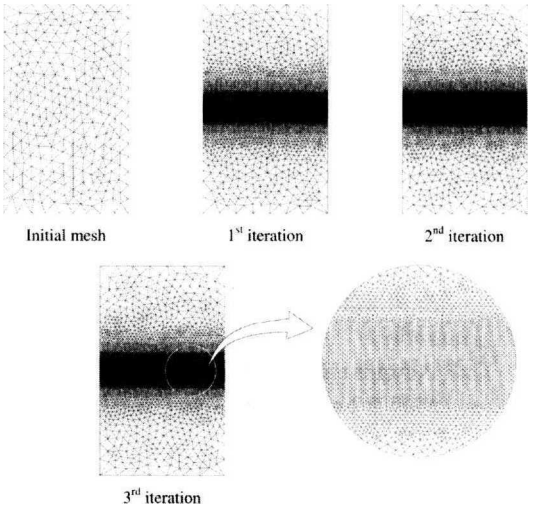

Fig. 1 Adaptive meshes along centerline of a rectangular domain

The specification of scale range and χ_{min}, χ_{max} have strong effects on the resulting meshes as shown in Fig. 1. Without the scale range, the mesh is composed of small elements concentrated around line a (see Fig. 2) with progressively larger elements outwards as $h_a<h_b$, h_c. Hence, a mesh consisting of relatively uniform elements in a wider centerline band of the domain may be generated. This mesh has better physical correlation with the behaviors of shocks. The scale range function sorts the nodal spacing values into prescribed intervals according to χ_{min} and χ_{max}. In each interval, the generated element sizes are relatively uniform.

Adaptive Meshes along a Diagonal of a Square Domain: The second example concerns with an adaptive mesh generation in a unit square domain. The element sizes are calculated by Eq. (7) where the constant α is set to 0.5 for this test case. Because this function generates both

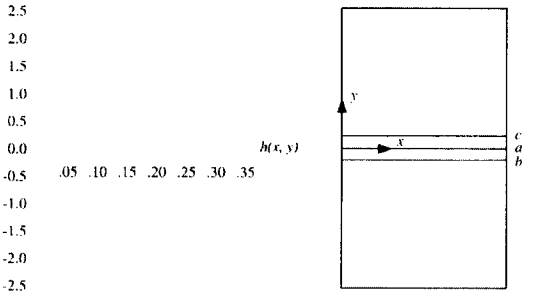

Fig. 2 Distribution of element sizes along the y direction

negative and positive values, only the positive values of this function are used to determine the element size by scaling into the new range of 0.001 and 0.2:

$$h(x, y)=2y(1-y)\left[\tan^{-1}\beta-\frac{\alpha(1-2x)}{\sqrt{2}(1+\beta^2)}+\frac{\alpha^2\beta x(1-x)}{2(1+\beta^2)^2}\right] +2x(1-x)\left[\tan^{-1}\beta-\frac{\alpha(1-2y)}{\sqrt{2}(1+\beta^2)}+\frac{\alpha^2\beta y(1-y)}{2(1+\beta^2)^2}\right] \quad (7)$$

where $\beta=\alpha[(x+y)/\sqrt{2}-0.8]$. Figure 3 shows the sequence of adaptive meshes generated by five iterations based on a coarse initial mesh. The value of mesh generation coefficients, α, β, χ_{min}, χ_{max} are 0.5, 0.6, 0.4, and 0.75, respectively. The combination of the values of χ_{min} and χ_{max}, narrows the band along the diagonal line with small elements.

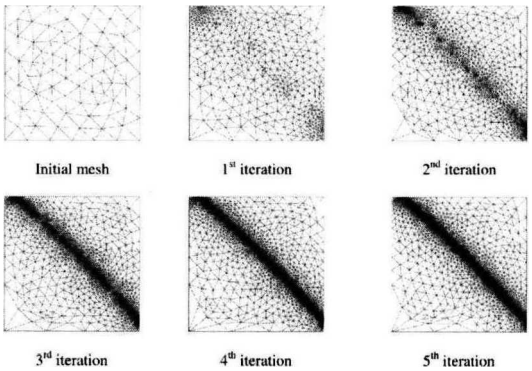

Fig. 3 Adaptive meshes along the diagonal of a square domain

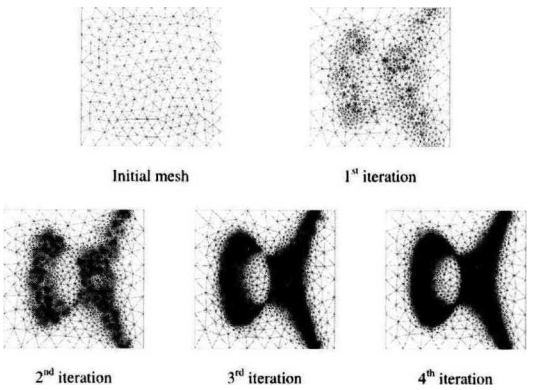

Fig. 4 An alpha-shape adaptive meshes in a square domain

An Alpha-Shape Adaptive Meshes in a Square Domain: The third example presents an alpha-shape adaptive mesh generation in a square domain. The alpha shape function (Borouchaki et al., 1997) is used to calculate element sizes in an 8×8 square domain:

$$h(x, y)=\begin{cases}\min(0.2(\lambda-1)^3+0.005, 1.0) & \text{if } \lambda\geq1\\ \min(0.2(\lambda-1)^2+0.01, 1.0) & \text{if } \lambda<1\end{cases} \quad (8)$$

where the value of parameter λ is determined from $x^3-y^2+2-3\lambda x=0$. Figure 4 shows the sequence of four adaptive meshes generated from a coarse initial mesh. The value of mesh generation coefficients, α, β, χ_{min}, χ_{max} are 0.5, 0.6, 0.5, and 0.85, respectively. The smaller elements are generated along the alpha-shape in the domain while larger elements are generated in the other regions.

For practical problems, the preferred values of α and β are 0.5 and 0.6, respectively (Karamete et al., 1997). In general, the acceptable ranges of these α and β values are 0.3~0.8, and 0.7~1.3, respectively. In addition, the values of 0.4 and 0.75 are chosen for χ_{min} and χ_{max}, respectively, for all high-speed compressible flow test cases presented later in this paper.

3. High-Speed Compressible Flow Solver

The performance of the Delaunay triangulation, the automatic point creation procedure, and the adaptive remeshing technique has been evaluated by applying to solve high-speed compressible flow problems. The Roe's flux-difference splitting method is widely used for compressible flow solutions due to its efficiency for providing solution accuracy. This section briefly explains the method and its flexibility for combining with adaptive unstructured meshes to further improve the solution accuracy.

Some certain problems for which the Roe's scheme may not provide correct solutions for the compressible Euler computation are presented in this section. Nonphysical numerical solutions may arise from the implementation of the one-dimensional upwinding numerical flux function

onto the multidimensional formulation. To avoid such solutions, a mixed entropy fix method that combines the entropy fix method of Van Leer et al. and the modified multidimensional dissipation method by Pandolfi and D'Ambrosio (2001) is proposed in this paper. Details of these entropy fix methods are presented herein and their performance are determined by test cases. All solutions in this section use the Roe's scheme with the first-order accuracy on structured triangular meshes.

3.1 Roe's flux-difference splitting scheme

The governing differential equations of the Euler equations for the two-dimensional inviscid flow are given by,

$$\frac{\partial \boldsymbol{U}}{\partial t}+\frac{\partial \boldsymbol{E}}{\partial x}+\frac{\partial \boldsymbol{G}}{\partial y}=0 \tag{9}$$

where $\boldsymbol{U}$ is the vector of conservation variables, $\boldsymbol{E}$ and $\boldsymbol{G}$ are the vectors of the convection fluxes in x and y directions, respectively. The perfect gas equation of state is in the form,

$$p=\rho e(\gamma-1) \tag{10}$$

where p is the pressure, ρ is the density, e is the internal energy, and γ is the specific heat ratio. By integrating Eq. (9) over a control volume, Ω, and applying the divergence theorem to the resulting flux integral,

$$\frac{\partial}{\partial t}\int_{\Omega}\boldsymbol{U}d\Omega+\int_{\partial\Omega}\boldsymbol{F}\cdot\hat{\boldsymbol{n}}dS=0 \tag{11}$$

where $\boldsymbol{F}$ is the numerical flux vector and $\hat{\boldsymbol{n}}$ is the unit normal vector of the cell boundary. The numerical flux vector at the cell interface between the left cell L and the right cell R according to the Roe's scheme (1981) is,

$$\boldsymbol{F}_n=\frac{1}{2}(\boldsymbol{F}_{nL}+\boldsymbol{F}_{nR})-\frac{1}{2}\sum_{k=1}^{4}\alpha_k|\lambda_k|\boldsymbol{r}_k \tag{12}$$

where α_k is the wave strength of the k^{th} wave, λ_k is the eigenvalue, and $\boldsymbol{r}_k$ is the corresponding right eigenvector. The eigenvalues in the above Eq. (12) are,

$$\lambda_k=\begin{bmatrix} V_n-a \\ V_n \\ V_n \\ V_n+a \end{bmatrix} \tag{13}$$

where V_n is the normal velocity, and a is the speed of sound at the cell interface.

3.2 The mixed entropy fix method

The original Roe's scheme previously described has been found to produce unphysical solutions of the Euler equations in some certain problems. These include the expansion shock from a flow over a step, and the carbuncle phenomenon of a flow over a blunt body. To avoid such unphysical solutions, the entropy fix methods (Harten, 1983; Van Leer et al., 1989; Pandolfi and D'Ambrosio, 2001; Lin, 1995; Sanders et al., 1998; Dechaumphai and Phongthanapanich, 2003) have been proposed and investigated. By numerical experiment, the Van Leer et al.'s entropy fix method can perform very well for flows with expansion shocks that contain sonic points such as flows over a forward facing step. Meanwhile, the Pandolfi and D'Ambrosio version of the H-correction entropy fix is suitable to correct the numerical instability from insufficient dissipation injected to the entropy and shear waves such as the flow over the blunt body problem. Thus, this paper proposes a mixed entropy fix method that combines the entropy fix method of Van Leer et al. and the modified multidimensional dissipation method by Pandolfi and D'Ambrosio, the modified H-correction, together by replacing the original eigenvalues as follows,

$$|\lambda_k|=\begin{cases} |\lambda_{1,4}| & ,\ |\lambda_{1,4}|\geq 2\eta^{VL} \\ \dfrac{|\lambda_{1,4}|^2}{4\eta^{VL}}+\eta^{VL} & ,\ |\lambda_{1,4}|<2\eta^{VL} \\ \max(|\lambda_{2,3}|,\ \eta^{PA}) & \end{cases} \tag{14}$$

where η^{VL} and η^{PA} are determined from,

$$\eta^{VL}=\max(\lambda_R-\lambda_L,\ 0) \tag{15}$$

$$\eta^{PA}=\max(\eta_2,\ \eta_3,\ \eta_4,\ \eta_5) \tag{16}$$

The values η_i, $i=2$ to 5 as shown in Figures 5(a)-(b) for both the structured and unstructured meshes are given by $\eta_i=0.5\max_k(|\lambda_{kR}-\lambda_{kL}|)$ where L and R denote the left and right elements, respectively.

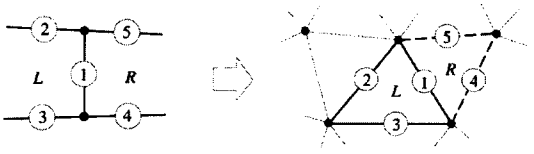

Fig. 5 Cell interfaces of: (a) structured uniform mesh; (b) unstructured triangular mesh

This mixed entropy fix method is equivalent to the Van Leer et al.'s entropy fix method in handling the acoustic waves (for $k=1$ and 4) and the Pandolfi and D'Ambrosio version of the H-correction entropy fix for the entropy and shear waves (for $k=2$ and 3). The mixed entropy fix method has been evaluated in this paper using three test cases involving expansion shocks, the carbuncle phenomenon, and the odd-even decoupling. These test cases highlight the performance of the proposed entropy fix method on problems with different flow phenomena on structured triangular meshes.

The carbuncle phenomenon: An unrealistic flow solution, the so-called carbuncle phenomenon, of a steady-state flow over a blunt body from the original Roe's scheme was first reported by Perry and Imlay (1988). Such phenomenon refers to a spurious bump on the bow shock near the flow center line ahead of the blunt body. The phenomenon is highly grid-dependent (Pandolfi and D'Ambrosio, 2001), but does not require a large number of grid points to appear (Gressier and Moschetta, 2000). Figures 6(a)-(f) show the computed density contours from the mixed entropy fix method using meshes of three different element aspect ratios. The enlarged views of the elements near the flow center line of the first, second, and the third meshes are also shown in the figures. The carbuncle phenomenon does not appear in all of these meshes with different element aspect ratios.

The Quirk's test (odd-even decoupling): Another test case is a mach 6 moving shock along odd-even grid perturbation in a straight duct (Quirk, 1994). The computational domain consists of a uniform triangular mesh with 800 and 20 equal intervals respectively along the axial

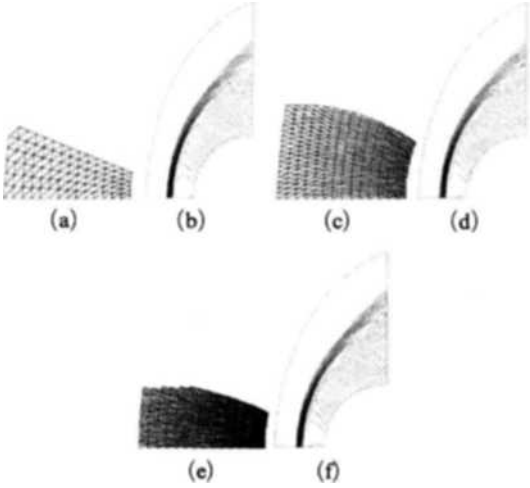

Fig. 6 Mach 15 flow over a blunt body, enlarged view of the mesh and computed density contours: (a)-(b) first mesh; (c)-(d) second mesh; and (e)-(f) third mesh

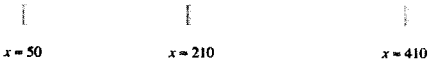

Fig. 7 Mach 6 moving shock along odd-even grid perturbation

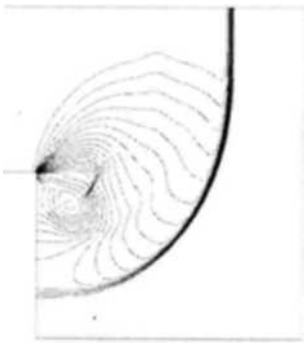

Fig. 8 Diffraction of a Mach 2 shock over a 90° corner

and the transverse directions of the duct. The grids along the duct centerline are perturbed in the transverse direction with a magnitude of $\pm 10^{-6}$. Figure 7 shows the computed density contours of the normal shock at three locations along the duct by the mixed entropy fix method that provides accurate shock resolution.

Shock diffraction: The last test case, the expansion shock problem, used to evaluate the nu-

merical instability is the diffraction of a Mach 2 shock moving over a 90° corner. Figure 8 shows the computed density contours obtained from the mixed entropy fix method. On the other hand, the original Roe's scheme could not provide proper solution due to the negative internal energy that occurs during the computation in the vicinity of the turning corner.

4. Higher-Order Extension and Application on Unstructured Triangular Meshes

4.1 Linear reconstruction for unstructured triangular mesh and temporal discretization

Solution accuracy from the first-order formulation described in the preceding section can be improved by implementing a higher-order formulation for both space and time. A higher-order spatial discretization is achieved by applying the Taylor' series expansion to the cell-centered solution for each cell face (Frink, 1994). For instance, the solutions at the midpoint of an element edge between node 1 and 2 can be reconstructed from,

$$\boldsymbol{q}_{J_{1-2}}=\boldsymbol{q}_C+\frac{\Psi_C}{3}\left[\frac{(\boldsymbol{q}_1+\boldsymbol{q}_2)}{2}-\boldsymbol{q}_3\right] \tag{17}$$

where $\boldsymbol{q}=[\rho\ u\ v\ p]^T$ consists the primitive variables of the density, the velocity components, and the pressure, respectively; $\boldsymbol{q}_C$ is the solution at the element centroid; $\boldsymbol{q}_n$, $n=1, 2, 3$ are the solutions at nodes. In this paper, the pseudo-Laplacian method proposed by Holmes and Connell (Holmes and Connell, 1989) is used to determine nodal quantities,

$$\boldsymbol{q}_n=\sum_{i=1}^{N}(w_i\boldsymbol{q}_{C,i})\Big/\sum_{i=1}^{N}w_i \tag{18}$$

where $\boldsymbol{q}_{C,i}$ are the surrounding cell-centered values of node n, w_i is the cell weights, and N is the number of the surrounding cells. The cell weights, w_i, may be differed significantly from unity for some severe distorted meshes as indicated in Ref.(Holmes and Connell, 1989), with suggestion for clipping all the weights in the range of 0 to 2. In this paper, the clipping of weights is slightly different by modifying only the value of weights of boundary meshes. If any weight becomes negative, its absolute value is used for simplicity. Several examples presented below have shown that such modification performs well. The Ψ_C in Eq. (17) represents the limiter for preventing spurious oscillation that may occur in the region of high gradients. In this study, Vekatakrishnan's limiter function (Vekatakrishnan, 1995) is selected.

The second-order temporal accuracy is achieved by implementing the second-order accurate Runge-Kutta time stepping method (Shu and Osher, 1988). To reduce computational effort, the local element time steps are used for steady-state analysis, while the minimum global time step based on the idea in Ref.(Linde and Roe, 1997) is used for the transient analysis.

4.2 Numerical evaluation

The higher-order extension of the Roe's scheme with the proposed entropy fix method described in the preceding section is evaluated by solving several test cases. The modified scheme is also combined with the adaptive meshing technique that generates unstructured triangular meshes for more complex flow phenomena. The selected test cases are: (1) Symmetric rarefaction wave, (2) Oblique shock reflection at a wall, (3) Mach 2 flow in a 15° channel, and (4) Mach 2 shock reflection over a wedge.

Symmetric rarefaction wave: The initial conditions of the flow on the left and right sides of the tube are given by $(\rho, u, p)_L=(7.0, -1.0, 0.2)$ and $(\rho, u, p)_R=(7.0, 1.0, 0.2)$. Such initial conditions are chosen (Linde and Roe, 1997) to produce vacumm at the central region. The 1.0×0.1 computational domain is divided into 400 and 40 equal intervals in the x and y directions, respectively, using all triangular elements. Figures 9(a)-(c) show the first order accurate computed density, pressure and u-velocity distributions along the tube length at time $t=0.3$ which are compared with the Steger-Warming FVS (Steger and Warming, 1981), AUSM (Liou and Steffen, 1993), HLLC (Toro et al., 1994),

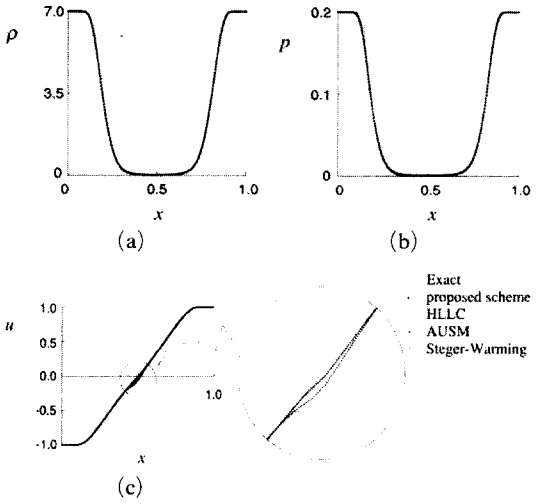

Fig. 9 Comparative exact and computed solutions at time $t=0.3$ for symmetric rarefaction wave problem $\vartheta(1)$: (a) density distributions; (b) pressure distributions; and (c) u-velocity distributions

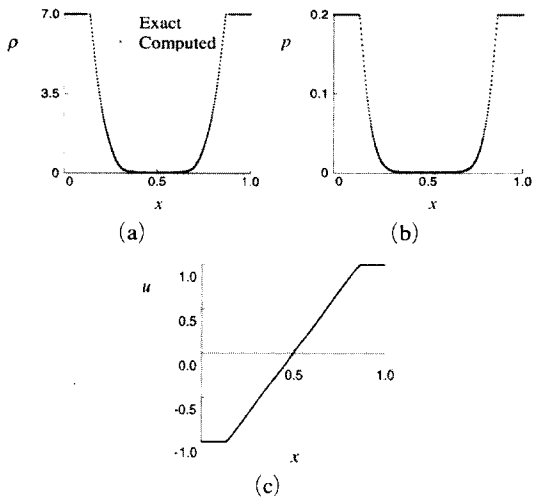

Fig. 10 Comparative exact and computed solutions at time $t=0.3$ for symmetric rarefaction wave problem $\vartheta(2)$: (a) density distributions; (b) pressure distributions; and (c) u-velocity distributions

and the exact solutions. The density and pressure distributions are nearly identical for the four schemes. But for the computed u-velocity, the AUSM and the HLLC schemes give less solution accuracy as compared to the Steger-Warming FVS and the proposed schemes in the vicinity of central region. This problem was repeated using the higher-order accurate scheme. Figures 10(a)-(c) show that such higher-order extension of Roe's scheme with the mixed entropy fix method can provide more accurate solution than its first-order solution.

Oblique shock reflection at a wall: The problem statement of an oblique shock reflection at a wall (Yee et al., 1985) on the domain 1.0×4.0 is presented in Fig. 11. The adaptive remeshing technique described is section 2.3 is used to generate adaptive unstructured triangular meshes. The procedure starts by creating a relatively uniform mesh as shown in Fig. 12(a). The fluid analysis is then performed to generate the corresponding solution such as the density contours as shown in Fig. 12(b). This flow solution is then used to generate an adaptive mesh to cluster small elements in the regions of high density gradients, and at the same time, to use larger

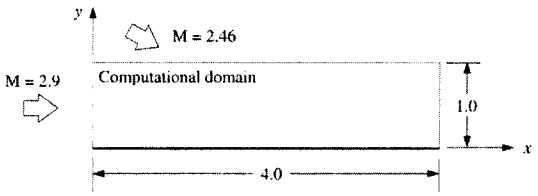

Fig. 11 Problem statement of an oblique shock reflection at a wall

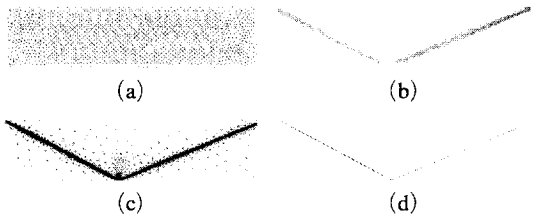

Fig. 12 An oblique shock reflection at a wall: (a)-(b) Initial mesh and the corresponding density contours; and (c)-(d) Third adaptive mesh and the corresponding density contours

elements on the other regions. The fluid analysis is then performed again to yield a more accurate solution. The entire process is repeated to

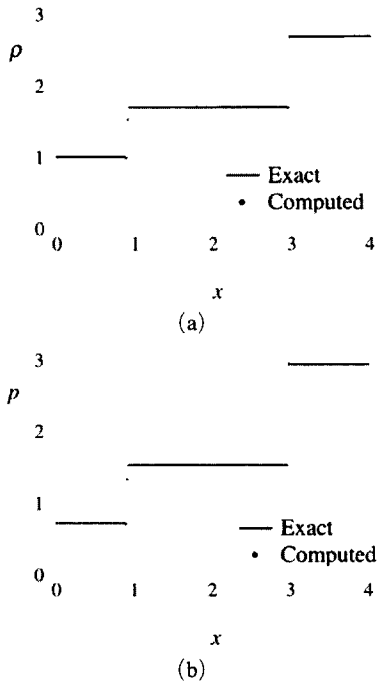

Fig. 13 Comparative solutions of an oblique shock reflection at a wall $\vartheta(2)$: (a) density distribution; and (b) pressure distribution

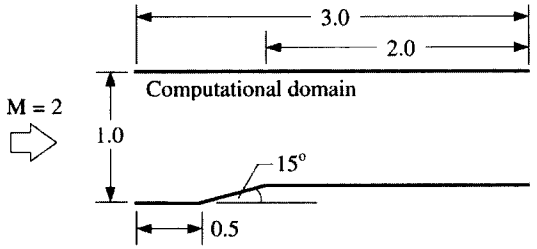

Fig. 14 Problem statement of a mach 2 flow in a 15° channel

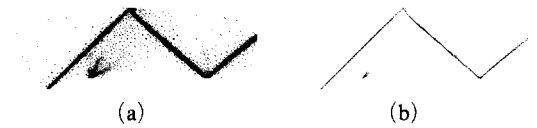

Fig. 15 Mach 2 flow in a 15° channel $\vartheta(1)$: (a) Third adaptive mesh; and (b) Density contours

Fig. 16 Mach 2 flow in a 15° channel $\vartheta(2)$: (a) Third adaptive mesh; and (b) Density contours

generate the third adaptive mesh and the corresponding solution as shown in Figs. 12(c)-(d). Figures 13(a)-(b) show comparative density and pressure distributions between the computed and exact solutions at $y=0.5$. The figures show the higher-order accurate scheme can capture abrupt change of the solutions across the shocks very well.

Mach 2 flow in a 15° channel: Both the first-order and higher-order Roe's schemes with the proposed entropy fix method are evaluated on unstructured meshes by using the problem of a Mach 2 flow in a 15° channel as presented in Fig. 14. The third adaptive mesh and its corresponding density contours computed by using the first-order scheme are shown in Figures 15 (a)-(b), respectively. The analysis of Mach 2 flow in the 15° channel is repeated but with the use of the higher-order scheme. The third adaptive mesh, and its corresponding density contours are shown in Figs. 16(a)-(b). These figures highlight the capability of the higher-order scheme for providing more detailed flow behavior, such as the stem generated from the shock impinging on the upper wall which could not be captured by the first-order scheme.

Mach 2 shock reflection over a wedge: The computational domain for a Mach 2 shock reflection over a wedge at 46 degrees (Takayama and Jiang, 1997) is illustrated in Figure 17. Figure 18 shows series of the transient adaptive meshes and the corresponding computed density contours at different time instants as the reflection shock starts to form over a wedge. The transient adaptive meshes consist of approximately 20,000 elements in early time before the normal shock reaches the wedge corner, and the number of elements are increased to approximately 28,000 at bottom right image of Fig. 18. The figures highlight the use of the higher-order accurate scheme on adaptive meshes to effectively obtain detailed flow solution.

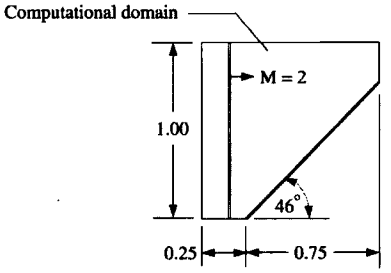

Fig. 17 Problem statement of a Mach 2 shock reflection over a wedge

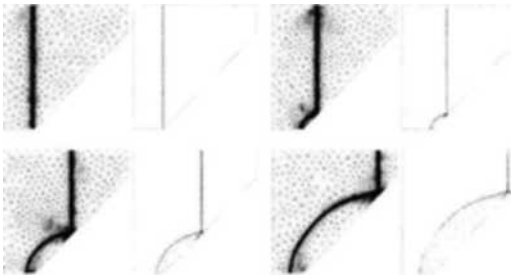

Fig. 18 Transient adaptive meshes and the computed density contours of a Mach 2 shock reflection over a wedge at four different stages of the computation $\vartheta(2)$

5. Conclusion

A two-dimensional adaptive Delaunay mesh generation algorithm and its application for high-speed compressible flow were presented. The adaptive remeshing technique was described in detail with the pseudo-code presented in object-oriented programming concept. To capture fast variations of the solution effectively, a new element size scaling function was introduced into the adaptive remeshing technique. The combined algorithm was evaluated by generating adaptive meshes for three examples with prescribed element size functions.

A mixed entropy fix method was proposed to improve numerical stability of the Roe's flux-difference splitting scheme for solving high-speed compressible flow problems. The method combines the entropy fixes by Van Leer et al. together with Pandolfi and D'Ambrosio. The method was then evaluated by several well-known test cases and it was found to eliminate unphysical solutions that may arise from the use of the original Roe's scheme. The method was also combined with an adaptive mesh generation technique to demonstrate its applicability for arbitrary unstructured meshes. The entire process was found to provide accurate solutions for both steady-state and transient flow test cases.

Acknowledgment

The authors are pleased to acknowledge the Thailand Research Fund (TRF) for supporting this research work.

References

Borouchaki, H., George, P. L. and Mohammadi, B., 1997, "Delaunay Mesh Generation Governed by Metric Specifications. Part II. Application," *Finite Elements in Analysis and Design*, Vol. 25, pp. 85~109.

Bowyer, A., 1981, "Computing Dirichlet Tessellations," *Computer Journal*, Vol. 24, pp. 162~166.

Dechaumphai, P. and Morgan, K., 1992, "Transient Thermal-Structural Analysis using Adaptive Unstructured Remeshing and Mesh Movement," Thermal Structures and Materials for High-Speed Flight, AIAA, Washington, D.C., pp. 205~228.

Dechaumphai, P. and Phongthanapanich, S., 2003, "High-Speed Compressible Flow Solutions by Adaptive Cell-Centered Upwinding Algorithm with Modified H-correction Entropy Fix," *Advances in Engineering Software*, Vol. 32, pp. 533~538.

Frey, W. H., 1991, "Mesh Relaxation : A New Technique for Improving Triangulations," *International Journal for Numerical Methods in Engineering*, Vol. 31, pp. 1121~1133.

Frink, N. T., 1994, "Recent Progress toward a Three-dimensional Unstructured Navier-Stokes Flow Solver," 32th Aerospace Sciences Meeting, Reno, Nevada, *AIAA Paper-94-0061*.

Gressier, J. and Moschetta, J. M., 2000, "Robustness versus Accuracy in Shock-wave Computations," *International Journal for Numerical*

Methods in Fluids, Vol. 33, pp. 313~332.

Harten, A., 1983, "High Resolution Schemes for Hyperbolic Conservation Laws," *Journal of Computational Physics*, Vol. 49, pp. 357~393.

Holmes, D. G. and Connell, S. D., 1989, "Solution of the 2D Navier-Stokes Equations on Unstructured Adaptive Grids," 9th Computational Fluid Dynamics Conference, Buffalo, New York, *AIAA Paper-89-1932-CP*.

Kang, H. K., Tsutahara, M., Ro, K. D. and Lee, Y. H., 2002, "Numerical Simulation of Shock Wave Propagation using the Finite Difference Lattice Boltzmann Method," *KSME International Journal*, Vol. 16, pp. 1327~1335.

Kang, H. K., Tsutahara, M., Ro, K. D. and Lee, Y. H., 2003, "Numerical Analysis of a Weak Shock Wave Propagating in a Medium using Lattice Boltzmann Method (LBM)," *KSME International Journal*, Vol. 17, pp. 2034~2041.

Karamete, B. K., Tokdemir, T. and Ger, M., 1997, "Unstructured Grid Generation and a Simple Triangulation Algorithm for Arbitrary 2-D Geometries using Object Oriented Programming," *International Journal for Numerical Methods in Engineering*, Vol. 40, pp. 251~268.

Lin, H. C., 1995, "Dissipation Additions to Flux-Difference Splitting," *Journal of Computational Physics*, Vol. 117, pp. 20~27.

Linde, T. and Roe, P. L., 1997, "Robust Euler Codes," *AIAA Paper-97-2098*, 13th Computational Fluid Dynamics Conference, Snowmass Village, CO.

Liou, M. S. and Steffen, C. J., 1993, "A New Flux Splitting Scheme," *Journal of Computational Physics*, Vol. 170, pp. 23~39.

Marchant, M. J. and Weatherill, N. P., 1993, "Adaptivity Techniques for Compressible Inviscid Flows," *Computer Methods in Applied Mechanics and Engineering*, Vol. 106, pp. 83~106.

Pandolfi, M. and D'Ambrosio, D., 2001, "Numerical Instabilities in Upwind Methods: Analysis and Cures for the 'Carbuncle' Phenomenon," *Journal of Computational Physics*, Vol. 166, pp. 271~301.

Perry, K. M. and Imlay, S. T., 1988, "Blunt-body Flow Simulations," 24th AIAA/SAE/ASME/ASEE Joint Propulsion Conference, Boston, MA, *AIAA Paper-88-2904*.

Phongthanapanich, S. and Dechaumphai, P., 2004, "Evaluation of Combined Delaunay Triangulation and Remeshing for Finite Element Analysis of Conductive Heat Transfer," *Transactions of the Canadian Society for Mechanical Engineering*, Vol. 27, pp. 319~340.

Probert, J., Hassan, O., Peraire, J. and Morgan, K., 1991, "An Adaptive Finite Element Method for Transient Compressible Flows," *International Journal for Numerical Methods in Engineering*, Vol. 32, pp. 1145~1159.

Quirk, J. J., 1994, "A Contribution to the Great Riemann Solver Debate," *International Journal for Numerical Methods in Fluids*, Vol. 18, pp. 555~574.

Roe, P. L., 1981, "Approximate Riemann Solvers, Parameter Vectors, and Difference Schemes," *Journal of Computational Physics*, Vol. 43, pp. 357~372.

Sanders, R., Morano, E. and Druguet, M. C., 1998, "Multidimensional Sissipation for Upwind Schemes: Stability and Applications to Gas Dynamics," *Journal of Computational Physics*, Vol. 145, pp. 511~537.

Shu, C. W. and Osher, S., 1988, "Efficient Implementation of Essentially Non-Oscillatory Shock-capturing Schemes," *Journal of Computational Physics*, Vol. 77, pp. 439~471.

Steger, J. L. and Warming, R. F., 1981, "Flux Vector Splitting of the Inviscid Gasdynamic Equations with Applications to Finite Difference Methods," *Journal of Computational Physics*, Vol. 40, pp. 263~293.

Takayama, K. and Jiang, Z., 1997, "Shock Wave Reflection over Wedges: a Benchmark Test for CFD and Experiments," *Shock Waves*, Vol. 7, pp. 191~203.

Toro, E. F., Spruce, M. and Speares, W., 1994, "Restoration of the Contact Surface in the HLL-Riemann Solver," *Shock Waves*, Vol. 4, pp. 25~34.

Van Leer, B., Lee, W. T. and Powell, K. G., 1989, "Sonic-Point Capturing," 9th Computational Fluid Dynamics Conference, Buffalo, New York, *AIAA Paper-89-1945-CP*.

Vekatakrishnan, V., 1995, "Convergence to

Steady State Solutions of the Euler Equations on Unstructured Grids with Limiters," *Journal of Computational Physics*, Vol. 118, pp. 120~130.

Watson, D. F., 1981, "Computing the n-Dimensional Delaunay Tessellation with Application to Voronoi Polytopes," *Computer Journal*, Vol. 24, pp. 167~172.

Yee, H. C., Warming, R. F. and Harten, A., 1985, "Implicit Total Variation Diminishing (TVD) Schemes for Steady-state Calculations," *Journal of Computational Physics*, Vol. 57, pp. 327~360.